Pure Appl. Geophys. 172 (2015), 885–899

DOI 10.1007/s00024-014-1016-3

Pure and Applied Geophysics

Runup of Nonlinear Long Waves in Trapezoidal Bays: 1-D Analytical Theory and 2-D Numerical Computations

M. W. Harris,[1] D. J. Nicolsky,[2] E. N. Pelinovsky,[3,4] and A. V. Rybkin[1]

Abstract—Long nonlinear wave runup on the coasts of trapezoidal bays is studied analytically in the framework of one-dimensional (1-D) nonlinear shallow-water theory with cross-section averaging, and is also studied numerically within a two-dimensional (2-D) nonlinear shallow water theory. In the 1-D theory, it is assumed that the trapezoidal cross-section channel is inclined linearly to the horizon, and that the wave flow is uniform in the cross-section. As a result, 1-D nonlinear shallow-water equations are reduced to a linear, semi-axis variable-coefficient 1-D wave equation by using the generalized Carrier–Greenspan transformation [Carrier and Greenspan (J Fluid Mech 1:97–109, 1958)] recently developed for arbitrary cross-section channels [Rybkin *et al.* (Ocean Model 43–44:36–51, 2014)], and all characteristics of the wave field can be expressed by implicit formulas. For detailed computations of the long wave runup process, a robust and effective finite difference scheme is applied. The numerical method is verified on a known analytical solution for wave runup on the coasts of an inclined parabolic bay. The predictions of the 1-D model are compared with results of direct numerical simulations of inundations caused by tsunamis in narrow bays with real bathymetries.

Key words: Wave run-up, shallow water wave equations, Carrier–Greenspan transformation, numerical simulation.

1. Introduction

The Aleutian megathrust, where the Pacific plate is being subducted underneath the North American plate, has delivered numerous great earthquakes and is considered one of the most seismically active tsunamigenic fault zones in the U.S. (Ruppert *et al.* 2007; Benz *et al.* 2011). The latest sequence of great earthquakes rupturing the Aleutian megathrust started in 1938 with a M8.3 earthquake west of Kodiak Island. Three consequent events; the M8.6 1957 Andreanof Island, the M9.2 1964 Alaska, and the M8.7 1965 Rat Island earthquakes ruptured almost the entire length of the megathrust. Tsunamis generated by these large earthquakes traveled several hours and impacted exposed shorelines across the Pacific Ocean (Gusiakov *et al.* 1997; NGDC 2013). The devastating 1964 tsunami struck the seaboard of southeast Alaska and then traveled into the narrow channels and canals further inland. The communities of Skagway and Haines located at the end of Lynn Canal were struck by 3.0 and 5.8 m waves during the 1964 event (NGDC 2013). It is believed that subduction of the Pacific plate still has the greatest potential to generate tsunamis that would affect Alaska (Dunbar and Weaver 2008). The impact of a tsunami depends on how well a community is prepared and on how efficient emergency managers can evacuate near-shore areas.

In the case of tsunamis, depending on the information bulletin issued by tsunami warning centers, it is recommended that emergency managers and harbor masters take action ranging from limiting waterfront access to full near-shore evacuation (Ewing 2011; Wilson *et al.* 2013). A quick and robust assessment of the incoming tsunami is paramount for identifying what type of preventative action to take. To help emergency managers evaluate the situation, the warning centers process all available data and provide a forecast of the potential inundation at selected sites (Tang *et al.* 2009). At other locations, the only information available may be near-shore tsunami height (Wilson *et al.* 2013). Thus, quick and efficient

[1] Department of Mathematics and Statistics, University of Alaska Fairbanks, Fairbanks, AK 99709, USA. E-mail: mharris15@alaska.edu
[2] Geophysical Institute, University of Alaska Fairbanks, Fairbanks, AK 99709, USA.
[3] Institute of Applied Physics, Nizhny Novgorod, Russia.
[4] Nizhny Novgorod State Technical University, Nizhny Novgorod, Russia.

estimates of the potential runup at locations where warning center forecasts are not yet available are important to select an appropriate evacuation procedure (R. Wilson, California Department of Conservation Agency and K. Miller, California Governor's Office of Emergency Services, personal communication 2014). Recent studies of the 2011 Tohoku tsunami suggest that the local bathymetry (U-shaped verses V-shaped) is a key component in predicting the local runup, with V-shaped bays having larger runup than U-shaped bays (Liu *et al.* 2013; Shimozono *et al.* 2012; Kim *et al.* 2013; Shimozono *et al.* 2014). Over-evacuation may result in heavy costs to businesses and potentially damage public confidence in response activities (Kiffer 2012; Wilson and Miller 2014).

The 2-D nonlinear shallow water theory is commonly used to predict the long wave propagation and inundation of coastal areas (Synolakis and Bernard 2006). In the case of narrow, long channels and fjords, the governing equations could be simplified into 1-D equations (Stoker 1957; Pelinovsky and Troshina 1994; Didenkulova and Pelinovsky 2011b; Rybkin *et al.* 2014). The mass and linear momentum conservation principles become

$$\frac{\partial S}{\partial t}+\frac{\partial}{\partial x}(uS)=0, \tag{1}$$

$$\frac{\partial u}{\partial t}+u\frac{\partial u}{\partial x}+g\frac{\partial H}{\partial x}=g\frac{\mathrm{d}h}{\mathrm{d}x}. \tag{2}$$

Here, $u=u(x,t)$ is the averaged cross-section velocity, $\eta=\eta(x,t)$, and $h=h(x)$ are the water displacement and unperturbed water depth along the main axis of the bay, respectively. The quantity $H(x,t)=\eta(x,t)+h(x)$ is called the total water depth, g is the acceleration of gravity, and $S(x,t)$ is the cross-section area of the bay. We assume that S is a function of total depth H only; as such, the bay cross-section does not change with distance. Wave geometry is shown in Fig. 1.

Carrier and Greenspan (1958) were the first to use a hodograph transformation to find an analytical solution to Eqs. (1–2) for the case of a sloping plane beach in a rectangular channel. One of the major results was a formula linking the height of the incident wave to the runup. More recently, Didenkulova and Pelinovsky (2011a) and Rybkin *et al.* (2014) built upon the ideas of Carrier and Greenspan and generalized the transformation for an inclined bay with an arbitrary cross-section. The final product is a transformation from the nonlinear Eqs. (1) and (2) into a linear second order equation with non-constant coefficients (Didenkulova and Pelinovsky 2011b; Rybkin *et al.* 2014). This model is described in Sect. 2.

The generalized linear equation has a strong singularity at the moving shoreline and this leads to some difficulties when computing the numerical solution of the transformed equation. In Sect. 3, we develop a semi-analytic numerical method using the generalized transform to simulate tsunami waves in trapezoidal bays. The proposed method is computationally inexpensive and provides bay runup estimates that can be approximated by trapezoidal cross-sections. Section 4 deals with verification of our numerical method in a bay for which an analytic solution is known (a bay with a parabolic cross-section). We then validate the developed method by comparing its numerical solution for a trapezoidalal cross-section bay against FUNWAVE, a 3D direct numerical method of solving Boussinesq equations. In Sect. 6, we discuss applicability of 1-D equations to tsunami waves in bays with real bathymetry.

2. *Generalized Carrier–Greenspan Transform*

In this section, we provide a brief review of the generalized transformation by Rybkin *et al.* (2014) for a linearly inclined bay with arbitrary cross-sections. Following Rybkin *et al.* (2014) we assume that the bay bathymetry is determined by function $Z=f(y)-h(x)$, where $f(y)$ describes the bay bathymetry across the primary axis and $h(x)$ is restricted to $h(x)=\alpha x$ for some bay slope α. We note that the Riemann invariants and corresponding characteristics have been found as $J_{\pm}=u\pm\int\sqrt{\frac{g}{S}\frac{\mathrm{d}S}{\mathrm{d}H}}\mathrm{d}H$ and $c_{\pm}=u\pm\sqrt{gS\frac{\mathrm{d}H}{\mathrm{d}S}}$.

Furthermore, it is shown that Eqs. (1) and (2) can be reformulated in terms of $I_{\pm}=J_{\pm}+g\alpha t$ as

$$\frac{\partial x}{\partial I_{\mp}}-c_{\pm}\frac{\partial t}{\partial I_{\mp}}=0, \tag{3}$$

Consequently, a new coordinate system (σ,λ) is defined in terms of the Riemann invariants, i.e., $\lambda=(I_{+}+I_{-})/2$ and $\sigma=(I_{+}-I_{-})/2$, or

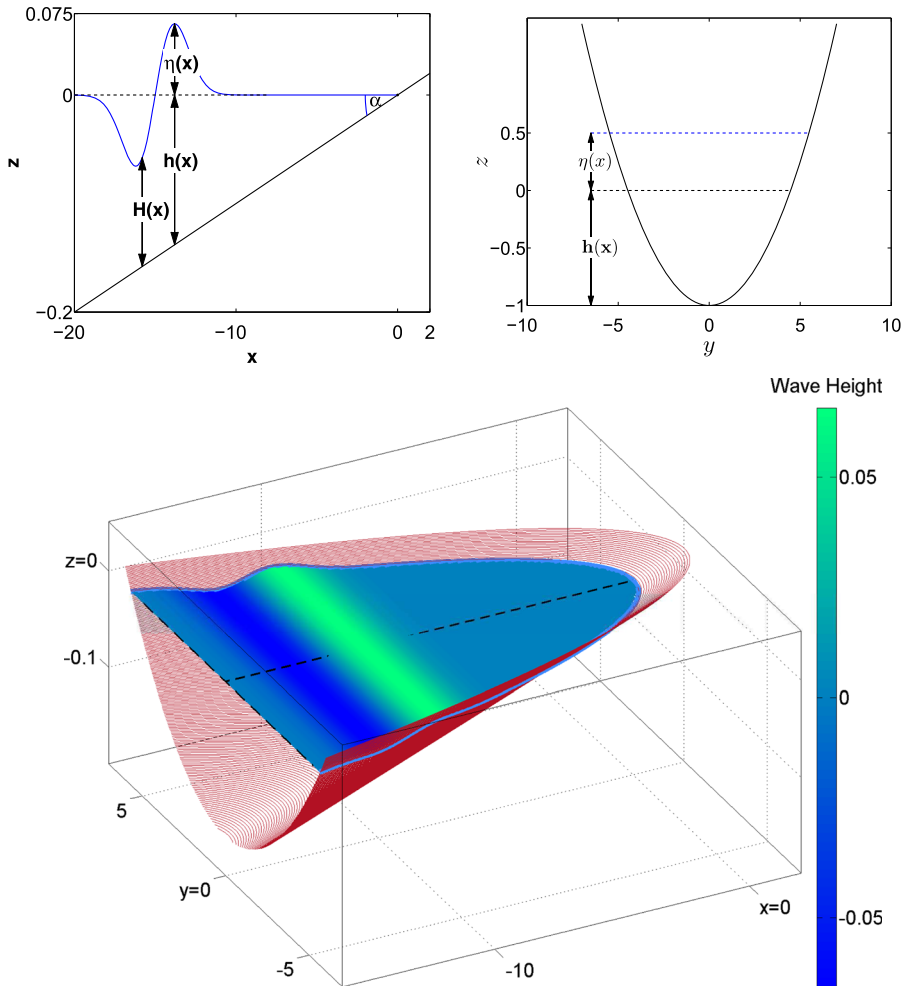

Figure 1
Top left a (x, z) cross-sectional view of the U-shaped bay, *top right* a (y, z) cross-sectional view of the U-shaped bay, and *bottom* a 3D view of the bay

$$\lambda = u + \alpha g t, \qquad \sigma = \int_0^H \sqrt{g} D(h) \mathrm{d}h, \tag{4}$$

where

$$D(H) = \frac{\partial}{\partial H} \sqrt{\ln S(H)}$$

The variable λ is related to time, while σ is associated with the spatial variable. Note that at the shoreline $H = 0$, and, thus, the shoreline location is associated with $\sigma = 0$. Therefore, σ is always non-negative, whereas x will become negative during the tsunami runup. If the initial water velocity $u_0(x, 0) = 0$, then $t = 0$ corresponds to $\lambda = 0$ for all x.

In order to exploit the convenient properties of the $\sigma - \lambda$ system, Rybkin *et al.* (2014) defined a function $F = F(\sigma)$ and the potential $\Phi = \Phi(\sigma, \lambda)$ such that

$$F(\sigma) = c_+ - c_- = \frac{2\sqrt{g}}{D(H(\sigma))}, \qquad u = \frac{\Phi_\sigma}{F}. \tag{5}$$

Equation (3), thus, transforms to

$$\Phi_{\lambda\lambda} - \Phi_{\sigma\sigma} - W(\sigma)\Phi_\sigma = 0, \qquad W(\sigma) = \frac{2 - F_\sigma}{F}. \tag{6}$$

After introducing two auxiliary functions $\varphi = \Phi_\lambda$ and $\psi = \Phi_\sigma$, it is easy to see that

$$\varphi_\lambda - \psi_\sigma - W\psi = 0. \tag{7}$$

Differentiating Eq. (7) in respect to σ and noting that $\varphi_\sigma = \psi_\lambda$, one obtains

$$\psi_{\lambda\lambda} = \psi_{\sigma\sigma} + (W\psi)_\sigma. \tag{8}$$

Finally, it was shown that the water disturbance η and velocity u can be derived through the following nonlinear transformation:

$$\begin{aligned} u &= \frac{\psi}{F},\ \eta = \frac{1}{2g}\left(\varphi - u^2\right), \\ x &= \frac{1}{2g\alpha}\left(\varphi - 2gH - u^2\right),\ t = \frac{\lambda - u}{\alpha g}. \end{aligned} \tag{9}$$

For the wave breaking condition of the physical wave, we are interested in the vanishing points of the Jacobian:

$$J = \frac{\partial(t,x)}{\partial(\sigma,\lambda)} = \frac{\sigma}{12g^2\alpha^2}\left[\left(1 - \frac{\partial u}{\partial\lambda}\right)^2 - \left(\frac{\partial u}{\partial\sigma}\right)^2\right]. \tag{10}$$

For a discussion of this Jacobian and the validity of the breaking condition, see Rybkin *et al.* (2014).

In order to solve (8), it is necessary to specify the initial and boundary conditions. Typically, the initial water disturbance η_0 and velocity u_0 are available in physical variables (x,t) and need to be transformed into the initial conditions in (σ,λ) coordinates. Exploiting (9), we obtain

$$\psi(\sigma,0) = u_0(x)F(\sigma), \quad \varphi(\sigma,0) = 2g\eta_0(x) + u_0^2(x), \tag{11}$$

where $x = x(\sigma)$ can be found by solving (9). Finding the initial conditions for an arbitrary $u_0(x)$ in sloping bays with an arbitrary cross section is still a open research question. There has, however, been some research in the case of a plane sloping beach. In particular, Kanoglu and Synolakis (2006) were able to find an analytic solution to the runup problem for an arbitrary u_0. As we will be approximating the solution via finite difference methods, the technique employed by Kanoglu and Synolakis (2006) can only be used when $\eta_0(x)$ is sufficiently small. For an arbitrary $\eta_0(x)$, we thus limit the scope of this paper by assuming that $u_0 = 0$, and, hence, after recalling that $\varphi_\sigma = \psi_\lambda$, we derive

$$\psi(\sigma,0) = 0, \quad \psi(\sigma,0)_\lambda = 2g\frac{\partial}{\partial\sigma}\left(\eta_0(x)\right). \tag{12}$$

The mapping between x and σ is determined by $H(\sigma) = H = \eta_0(x) - \alpha x$. To define the boundary condition at $\sigma = 0$, we note that $F(0) = 0$, and since the water velocity $u = \psi/F$ needs to be bounded, we impose

$$\psi(0,\lambda) = 0. \tag{13}$$

At the other boundary, $\sigma = \sigma_1$, such that $\sigma_1 \gg 1$ and $W \approx 0$. Consequently Eq. (8) can be approximated by the linear wave equation $\psi_{\lambda\lambda} = \psi_{\sigma\sigma}$. Therefore, a non-reflective boundary condition for (8) at $\sigma = \sigma_1$ can be approximated via

$$\psi_\lambda(\sigma_1,\lambda) = -\psi_\sigma(\sigma_1,\lambda). \tag{14}$$

In fact, these formulas are valid for bays with arbitrary cross-sections. In the next section, these boundary conditions will be applied to an inclined bay with a trapezoidal cross-section.

3. Numerical Algorithm

An analytical solution of Eq. (8) is currently only known for the following cases of bay bathymetry. Synolakis (1987) developed an analytical solution for soliton dynamics in a sloping bay with an infinite plane cross-section, i.e., $f(y) = \text{const}$, and Didenkulova and Pelinovsky (2011a) derived a formula to compute the runup in a sloping bay with parabolic cross-sections, i.e., $f(y) = y^2$. Recently, an analytical solution for water dynamics in a sloping bay with a cross-section defined by $f(y) = |y|^\alpha$ for $\alpha > 0$ was found by Garayshin (2013). For all other cases of $f(y)$, one should rely on solving Eq. (8) numerically.

We now present an efficient and robust numerical technique based on the finite difference method (Fletcher 1991) to simulate wave runup at the head of a sloping beach. As an example, we consider a wave propagating in a trapezoidal channel with the geometry shown in Fig. 2. The quantity y_0 is half of the base length, and β is the slope of the lateral walls. For this particular combination of parameters, we determine that the parameter D in (4) is expressed by

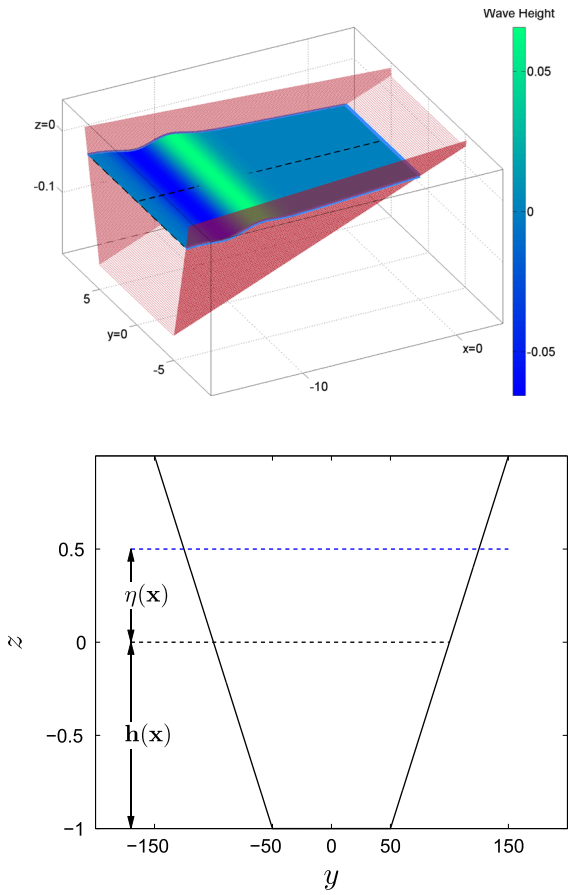

Figure 2
Top a schematic view of a wave propagating in a trapezoidal beach with lateral wall slope $\beta = 1/2$, a *bottom* width of $2y_0 = 100$ m, and a beach inclination of $\alpha = 0.01$. *Bottom* a transverse cross-section of the bay

$$D = \sqrt{\frac{H + \beta y_0}{H^2 + 2\beta y_0 H}}.$$

Note that when $H \to 0$, according to (4) we obtain $\sigma \to \sqrt{H}$, and hence $\lim_{\sigma\to 0} F = 0$. Therefore, from its definition, we have $\lim_{\sigma\to 0} W = \infty$, and, thus, one of the difficulties in solving (8), or

$$\psi_{\lambda\lambda} = \psi_{\sigma\sigma} + (W\psi)_\sigma$$

by a finite difference scheme lies in choosing an appropriate formulation for the numerical scheme near $\sigma = 0$. Here, we decide to re-formulate the above equation as

$$\psi_{\lambda\lambda} = \psi_{\sigma\sigma} + W\psi_\sigma + W_\sigma\psi. \tag{15}$$

This formulation facilitates enforcement of the boundary condition $\psi(0,\lambda) = 0$ at the origin and allows for the discretization of all spatial derivatives by second order central differences (Fletcher 1991).

Because the Courant–Friedrichs–Lewy (CFL) stability condition (Courant *et al.* 1928) imposes severe requirements on the time step at the origin, if Eq. (15) is solved by an explicit finite difference scheme, we choose to apply an implicit method to (15) (Fletcher 1991). To compute the temporal derivative, we employ the second order central difference formula. The boundary condition (14) is discretized by first order one sided differences in time and space and the boundary (13) is computed directly.

A numerical scheme for a second order partial differential equation (PDE) requires knowledge of the initial condition at two consecutive time steps. The initial condition $\psi(\sigma,0) = 0$ is readily available. To obtain an approximation to ψ at the second time step, i.e., at $\lambda = \Delta\lambda$, we employ the Taylor series expansion

$$\begin{aligned}\psi(\sigma,\Delta\lambda) &= \psi(\sigma,0) + \Delta\lambda\psi_\lambda(\sigma,0) + \psi_{\lambda\lambda}(\sigma,0)\Delta\lambda^2/2 + O(\Delta\lambda^3)\\ &= \psi(\sigma,0) + 2g\Delta\lambda\eta_\sigma(\sigma,0) + 0 + O(\Delta\lambda^3)\\ &= \psi(\sigma,0) + 2g\Delta\lambda\eta_\sigma(\sigma,0) + O(\Delta\lambda^3).\end{aligned} \tag{16}$$

Note that $\psi(\sigma,\Delta\lambda)$ can be approximated with third order accuracy and our numerical scheme has at least a second order of accuracy in space and time.

Once the solution ψ is found at the set of points $\{k\Delta\sigma, l\Delta\lambda\}_{k=0,l=0}^{n,m}$, where $\Delta\sigma$ and $\Delta\lambda$ are the spatial and temporal discretization intervals for non-physical variables, we compute φ at the same points by employing (7) as follows:

$$\varphi_\lambda = \psi_\sigma + W\psi.$$

Here, the temporal derivative φ_λ is discretized by a forward first order finite difference, while ψ_σ is computed by a central second order difference to preserve overall accuracy of the numerical calculations. Finally, once the values of $\varphi(k\Delta\sigma, l\Delta\lambda)$ and $\psi(k\Delta\sigma, l\Delta\lambda)$ are computed, we apply the inverse transform equations (9) and consecutively compute η as well as u at some set of points $\{x,t\}_{kl}$. We emphasize that the set $\{x,t\}_{kl} = \frac{1}{2g\alpha}\varphi(k\Delta\sigma, l\Delta\lambda)$ does not have a uniform stepping in both the x and t

directions, since the mapping from (σ, λ) to (x, t) is nonlinear. Thus, in order to compute profiles of the water height η at constant time, we employ the Delaunay triangulation algorithm in MATLAB (2011) and linearly interpolate (η, u) between the nodes $\{x, t\}_{kl}$.

The choice of using Delaunay triangulation to transform the solution from $(k\Delta\sigma, l\Delta\lambda)$ to $\{x, t\}_{kl}$ is much faster than the Newton-Raphson method employed by KANOGLU (2004) and KANOGLU and SYNOLAKIS (2006). Finally, we note that there is a small cost to accuracy in the choice to use Delaunay triangulation over the Newton-Raphson method. In order to get a fast forecast, we believe that Delaunay triangulation is sufficiently accurate.

To find $\varphi(k\Delta\sigma, l\Delta\lambda)$ and $\psi(k\Delta\sigma, l\Delta\lambda)$, we must find $F(\sigma)$ and $W(\sigma)$ for the bay in question at uniformly spaced points $\{k\Delta\sigma\}$. First, we note that the function F can be explicitly obtained in terms of H, i.e., by formula (5). Since $F \to 0$ when $H \to 0$, the function F is prone to numerical error in the near shore. To overcome this potential issue, we develop a numerical method to accurately find $H_k = H(\sigma_k)$, where $\sigma_k = k\Delta\sigma$.

We will now give an example of our method to find $F_k = F(\sigma_k)$ for a sloping bay with trapezoidal

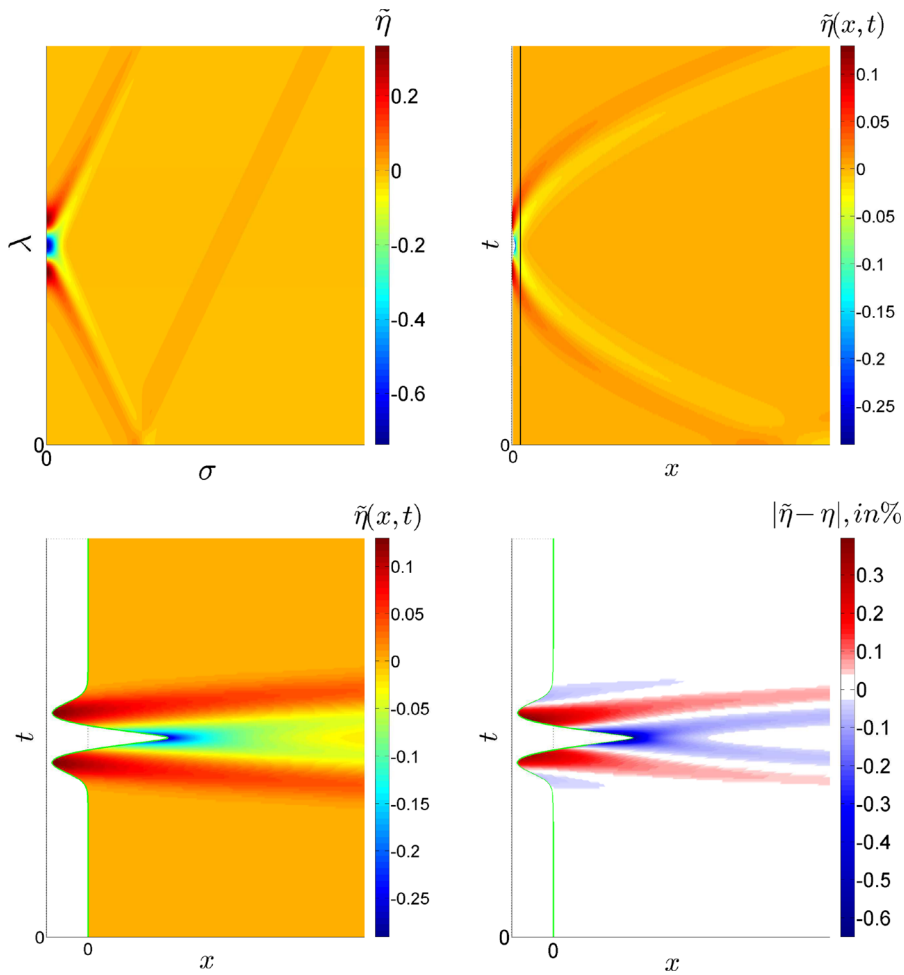

Figure 3

Top left numerically computed wave dynamics in non-physical coordinates (σ, λ). The shoreline is fixed at $\sigma = 0$. *Top right* numerically computed wave dynamics in physical coordinates (x, t). *Bottom left* shoreline dynamics of the physical wave by restricting the x axis to $[-1.5, 20]$. The shoreline varies around $x = 0$. *Bottom right* discrepancy between the analytical and numerical solution in the physical coordinates. The maximum errors occur at the runup (0.35 %) and rundown (0.65 %)

cross-sections, a base length $2y_0$, and wall slope β. By the definition of σ in Eq. (4), for the trapezoidal bay we obtain

$$\sigma_k = \sqrt{2g}\int_0^{H_k}\sqrt{\frac{h+\beta y_0}{h^2+2\beta y_0 h}}\,\mathrm{d}h.$$

Thus, for a given σ_k, we need to find H_k such that

$$G(H_k;\sigma_k) = \sigma_k - \sqrt{2g}\int_0^{H_k}\sqrt{\frac{h+\beta y_0}{h^2+2\beta y_0 h}}\,\mathrm{d}h = 0.$$

Solutions to $G(H_k;\sigma_k)=0$ can be found by using the Newton-Raphson method. Once $H_k = H(\sigma_k)$ is known, we calculate $F_k = F(H_k)$ according to (5). Exploiting the chain rule, we similarly obtain values of F_σ at $\{\sigma_k\}$ and thus compute $W_k = W(\sigma_k)$. It is notable that we only use the Newton-Raphson method to calculate F_k and W_k and not the time series at a specific location or spatial variation at a specific time as Synolakis and others have done (Synolakis 1987).

Finally, our algorithm for calculating wave dynamics is as follows

1. Given σ_k, compute H_k in order to find F_k, $(F_\sigma)_k$ and finally W_k.
2. Setup the initial condition $\psi(\sigma_k,0)$ according to (12).
3. Compute $\psi(\sigma_k,\lambda_1)$ at the second time step $\lambda_1 = \Delta\lambda$ according to (16).
4. Find $\psi(\sigma_k,\lambda_l)$ for consecutive time steps $l\geq 2$ according to the presented finite difference method (8).
5. Compute $\varphi(\sigma_k,\lambda_l)$ for $k,l\geq 1$ according to expression (7).
6. Use $\varphi(\sigma_k,\lambda_l)$, $\psi(\sigma_k,\lambda_l)$, F_k, and H_k to find $u(x_k,t_l)$, and $\eta(x_k,t_l)$ via (9).
7. Interpolate $\eta(x_k,t_l)$, $u(x_k,t_l)$ to uniformly spaced points (x,t) and find the values of runup R_u and rundown R_d.

4. Verification in a Parabolic Bay

In this section, we verify the accuracy of the numerical scheme by comparing the numerical solution to its analytical counterpart in the case of a parabolic bay given by cross sections $f = y^2$. Didenkulova and Pelinovsky (2011a) have shown that for the initial N-wave profile given by

$$\eta(\sigma,0) = \frac{2A(\sigma-\sigma_0)}{2gp^2}\mathrm{e}^{-(\sigma-\sigma_0)^2/p^2},$$

where A is the wave height, p is the wave length, and σ_0 represents the distance of the wave from the shore, the D'Alembert solution to (8) is

$$\Phi(\sigma\geq 0,\lambda) = \frac{A}{\sigma}\Big[\mathrm{e}^{-(\sigma+\lambda-\sigma_0)^2/p^2} - \mathrm{e}^{-(\sigma-\lambda-\sigma_0)^2/p^2} + \mathrm{e}^{-(\sigma+\lambda+\sigma_0)^2/p^2} - \mathrm{e}^{-(\sigma-\lambda+\sigma_0)^2/p^2}\Big].$$

Thus, in order to test the accuracy of our algorithm, we select an initial profile with $A=0.5$, $p=1.5$ and $\sigma_0 = 15$. Figure 1 shows the initial wave profiles in a parabolic bay with a bay slope of $\alpha = 0.01$. The propagation of the solitary wave towards the shore and its reflection from it is depicted in Fig. 3. The properties stated earlier about wave behavior in a non-physical system can clearly be seen. In the transformed non-physical system, the characteristics of the wave are linear, see Fig. 3, while the characteristics are curved for the system in the original physical coordinates. Also, notice that the solution is defined for all $\sigma\geq 0$; i.e., the shoreline is at $\sigma = 0$, whereas the shoreline moves with the wave height in physical coordinates (x,t) and the largest deviations of the shoreline from its initial position occurs at runup and rundown. Finally, the bottom right plot in Fig. 3 shows the absolute value of the difference between the numerical and analytic solutions in (x,t) coordinates. The largest error occurs at maximum run-up and minimum run-down.

For a parabolic sloping bay it is analytically derived that the values of run-up and rundown are $R_u = 8A\mathrm{e}^{-3/2}/3p^2$, and $R_d = -4A/3p^2$, respectively. For the above-mentioned values of A,p,σ_0, we have that the maximum wave run-up is $R_u \approx 0.1322$ and the minimum wave run-down is $R_d \approx -0.2963$. We will denote the computed run-up/run-down by $\tilde{R}_u$ and $\tilde{R}_d$, respectively. Tables 1 and 2 list the relative error in the computed run-up and run-down for several different combinations of $\Delta\lambda$ and $\Delta\sigma$, respectively. In both tables, it is notable that the error decreases

Table 1

Relative error $\|R_u - \tilde{R}_u\|/R_u$ in the run-up for different values of $\Delta\lambda$ and $\Delta\sigma$ values

Model run-up error with $(\Delta\lambda, \Delta\sigma)$	$\Delta\sigma = 1$	$\Delta\sigma = 0.1$	$\Delta\sigma = 0.01$	$\Delta\sigma = 0.005$
$\Delta\lambda = 1$	0.897372	0.896429	0.896429	0.896429
$\Delta\lambda = 0.1$	0.722520	0.690126	0.686332	0.686299
$\Delta\lambda = 0.01$	0.295066	0.178941	0.156491	0.156278
$\Delta\lambda = 0.001$	0.213095	0.085676	0.021997	0.021711
$\Delta\lambda = 0.0001$	0.204251	0.006944	0.004869	0.004573

Table 2

Relative error $\|R_d - \tilde{R}_d\|/R_d$ in the rundown for different values of $\Delta\lambda$ and $\Delta\sigma$ values

Model run-down error with $(\Delta\lambda, \Delta\sigma)$	$\Delta\sigma = 1$	$\Delta\sigma = 0.1$	$\Delta\sigma = 0.01$	$\Delta\sigma = 0.005$
$\Delta\lambda = 1$	0.959926	0.959926	0.959901	0.959900
$\Delta\lambda = 0.1$	0.823982	0.718481	0.716881	0.716866
$\Delta\lambda = 0.01$	0.685179	0.180632	0.171168	0.171078
$\Delta\lambda = 0.001$	0.663355	0.032658	0.019835	0.019714
$\Delta\lambda = 0.0001$	0.661000	0.015407	0.002167	0.002042

rapidly as we decrease both the $\Delta\sigma$ and the $\Delta\lambda$ values together. The effect of decreasing $\Delta\lambda$ on the error is greater than the effect of $\Delta\sigma$. This is primarily because our model is overall first order in computing φ in respect to $\Delta\lambda$ but quadratic in terms of $\Delta\sigma$; thus, when decreasing $\Delta\sigma$ (with $\Delta\lambda = \text{const.}$), we converge to the solution much quicker than when we decrease $\Delta\lambda$ (with $\Delta\sigma = \text{const.}$). Another property of our method that cannot be ignored is the fact that the maximum runup and minimum rundown times are not known but their spatial location is always at the moving shoreline ($\sigma = 0$). Thus, by decreasing $\Delta\lambda$ we are increasing the number of time samples where we compute the potential maximum runup/minimum rundown.

5. Validation in a Trapezoidal Bay

In this section, we test the proposed algorithm in the case of propagation and runup of waves in narrow bays with a trapezoidal profile. As noted earlier, the analytical solution to Eq. (8) for the case of wave propagation in bays with trapezoidal cross-sections is not yet available. Therefore, in order to validate our numerical algorithm, we compare it against the well-establish numerical model—FUNWAVE—which is considered to to be verified and validated by Tehranirad *et al.* (2012a, b) according to an exhaustive suite of tests proposed by Synolakis *et al.* (2008). We note that FUNWAVE employs a total variation diminishing finite volume scheme (Toro 2009) along with adaptive Runge-Kutta time stepping (Gottlieb *et al.* 2001) to model the propagation of the water waves. The interested reader can consult Shi *et al.* 2012 for further details about the FUNWAVE model. It is important to mention that FUNWAVE gives the user the option to take into account the wave dispersion (Shi *et al.* 2012), which is absent in Eqs. (1)–(2). Thus, for the validation of our method, we restrict FUNWAVE to non-dispersive behavior in our validation.

We assume an initial wave that approximates a disturbance caused by a small submarine land slump at the head of the fjord. Typically, if some ground material fails at the head of the bay, the material then slides down along the fjord wall and consequently generates an N-shaped wave with a leading depression. A conceptual picture of a landslide-generated wave is shown in Fig. 4. The initial and final positions of the slide are marked by letters A and B, respectively.

To test our proposed model, we assume an initial N-shaped wave with an amplitude of 10 cm has formed at the mouth of the narrow, rather steep glacial fjords typical of those found in Alaska (CITE), south-central Chili (Fritz *et al.* 2011b), and also in the Pago Pago bay in American Samoa (Fritz *et al.* 2011a; Didenkulova 2013); i.e., a trapezoidal bay with wall slope $\beta = 1/2$ and bottom slope $\alpha = 0.05$. The shoreline at the head of the bay is assumed to be 100 m, i.e., $y_0 = 50$. The distance from the center of the N-wave to the shore is assumed to be 1,000 m. The geometry of the idealized channel and wave profile are shown in Fig. 2.

In FUNWAVE, we simulate the propagation and runup of the same N-shaped wave with the trapezoidal bay in Fig. 2. When the dispersive effects are turned off, FUNWAVE solves the classical 2-D shallow water equations, while the proposed semi-analytical model computes the cross-section averaged

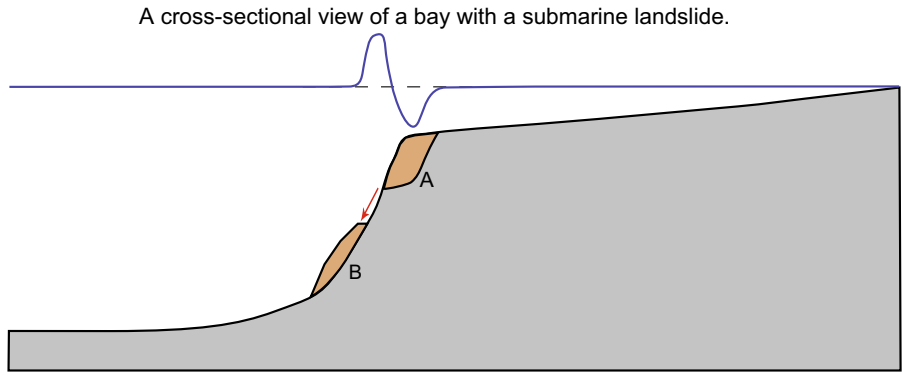

Figure 4
Schematic description of a submarine landslide. The landslide quickly moves material from its original location (*A*) to its resiting location (*B*). This movement typically generates an N-wave

characteristics of the flow. We decide to compare the results of the semi-analytical model with the results of FUNWAVE along the dashed line at the middle of the bay (see Fig. 2).

Figure 5 compares the water level, η, computed by the semi-analytical model and FUNWAVE [at $(y = 0)$]. Notice the discrepancy between the two models results for certain time periods. The top plot shows the waves as they approach the beach. The second plot from the top shows the minimum run-down that the waves achieve. At these points, there is minimal difference between the two model results. As shown in the third plot, 10 s after the waves reach the minimum run-down the simulated waves do not match up at the shore. In the fourth plot, the waves have reached their maximum run-up. Note that at this point, the two models predict nearly the same wave behavior. As the wave continues to propagate the discrepancy returns as shown in the fifth plot. Finally, at the bottom plot, after the wave reflection from the shore, the discrepancy is still present but not as large as it was at the shoreline. Despite the discrepancy, the models agree on the time and give approximately the same max runup magnitude (0.9236 vs. 0.9500 cm in FUNWAVE)/min rundown (-0.4753 vs. -0.4069 cm in FUNWAVE).

Finally, we compare prediction of the runup and rundown characteristics. Tables 3 and 4 demonstrate convergence of the computed runup and rundown amplitudes in the simulations with the semi-analytic model. In this table, one can see the apparent linear convergence in respect to $\Delta\lambda$ and quadratic convergence in respect to $\Delta\sigma$. The values of runup and rundown amplitudes obtained with the FUNWAVE model are provided in the table captions. Considering the significant differences between the two models, we determine that the predictions of the runup/rundown for the two models are close to each other, having 2.8 percent relative error in their runup values and 15.2 percent relative error in their rundown values.

6. *Long Wave in a Natural Bathymetry*

In this section, we analyze the capability of the developed model to simulate runup of geophysical tsunamis in natural bays and fjords. As an example of a real world fjord, we select Shotgun Cove—a fjord in Prince William Sound—located near the city of Whittier in south-central Alaska. To test our semi-analytical approach, the realistic fjord bathymetry is approximated by a canal with a trapezoidal cross-section. We then compare our results to those obtained with two different FUNWAVE setups in the realistic bathymetry—one without dispersive terms and one with dispersive terms. For the sake of convenience, we call the semi-analytical experiment "idealized," whereas the experiments where we consider FUNWAVE will be called "realistic."

The bathymetry at the head of Shotgun Cove is shown in Fig. 6. The digital elevation model for Shotgun Cove was assembled by the National Geophysics Data Center (Caldwell *et al.* 2009) and was re-gridded to the spatial resolution of 1.5 m. Note

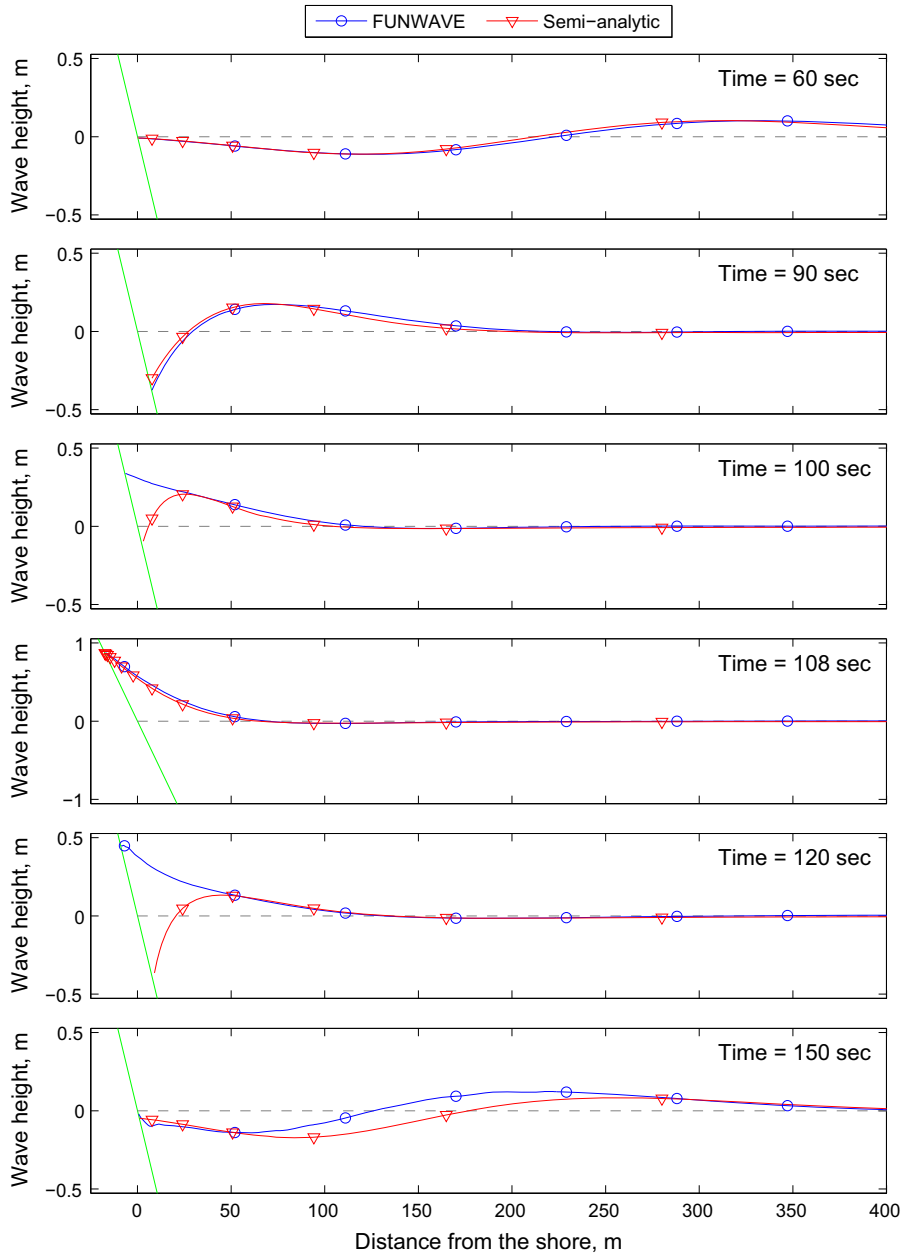

Figure 5
Comparison of the water level computed by the semi-analytic and FUNWAVE models

that Shotgun Cove consists of a gently sloping narrow channel connected via a steeply sloped part of the bay to a much deeper flat channel. Figure 6 displays the bathymetry profiles of the channel and locations of these profiles are marked by the green dotted lines. The zero distance corresponds to the shore at the south-west end of the channel. The bathymetry along the dotted lines exhibit a similar linear trend up to the depth of 10 m; the bathymetry then steeply declines as the channel connects to a much deeper part of Shotgun Cove. Therefore, in the idealized numerical experiment we hypothesize that the channel can be approximated by a 1 km-long trapezoidal channel with an inclination $\alpha = 0.01$. The computational

Table 3

Convergence of the $\tilde{R}_u$ computed by the semi-analytical model

Model Run-up with $(\Delta\lambda, \Delta\sigma)$	$\Delta\sigma = 1$	$\Delta\sigma = 0.1$	$\Delta\sigma = 0.01$	$\Delta\sigma = 0.005$
$\Delta\lambda = 1$	0.1890	0.1910	0.1910	0.1910
$\Delta\lambda = 0.1$	0.6900	0.7205	0.7209	0.7209
$\Delta\lambda = 0.01$	0.8473	0.8994	0.9001	0.9001
$\Delta\lambda = 0.001$	0.8662	0.9207	0.9214	0.9215
$\Delta\lambda = 0.0001$	0.8682	0.9229	0.9236	0.9236

Note that the rundown in the FUNWAVE simulation is 0.9500 cm

Table 4

Convergence of $\tilde{R}_d$ computed by the semi-analytical model

Model Run-down with $(\Delta\lambda, \Delta\sigma)$	$\Delta\sigma = 1$	$\Delta\sigma = 0.1$	$\Delta\sigma = 0.01$	$\Delta\sigma = 0.005$
$\Delta\lambda = 1$	−0.0998	−0.1000	−0.1000	−0.1000
$\Delta\lambda = 0.1$	−0.3694	−0.3643	−0.3643	−0.3643
$\Delta\lambda = 0.01$	−0.4774	−0.4614	−0.4613	−0.4613
$\Delta\lambda = 0.001$	−0.4916	−0.4741	−0.4740	−0.4740
$\Delta\lambda = 0.0001$	−0.4931	−0.4754	−0.4753	−0.4753

Note that the rundown in the FUNWAVE simulation is −0.4069 cm

domain for the so-called realistic numerical experiment is shown in Fig. 6 by the dashed black line.

In the realistic experiments, the long wave enters the computation domain through the upper boundary, shown in Fig. 6. The wave height gradually increases from 0 to 0.1 m in about 100 s. A profile of the incident wave at the mouth of the channel, along the line segment AB marked in Fig. 6, after $t = 100$ s is shown in Fig. 7. The wave propagates along the channel and then floods the head of the fjord. It takes about 1 CPU hour to simulate the propagation and runup using FUNWAVE. One of the outputs of the FUNWAVE model is the computed maximum wave height. The left plot in Fig. 8 shows the maximum attained wave height in the computation domain. We emphasize that the runup height at the head of the channel is about 0.5 m, about five times larger than the incident wave height at the mouth of the channel.

In the idealized experiment, we numerically match the simulated wave profile and set it at approximately the same distance from the shore as in the realistic experiment at $t = 100$ s. Since the wave propagates towards the shore, we supplement the initial small vertical disturbance η_0 with non-zero velocity $u_0 \approx -\eta_0\sqrt{g/h}$ given by KANOGLU and SYNOLAKIS (2006). The non-zero velocity is then utilized along with the first equation in (11) to find an approximation for $\psi(\sigma, 0)$ by the following formula:

$$\psi_0(\sigma, 0) \approx -\eta_0(x)\sqrt{\frac{g}{\alpha x}}F(\sigma).$$

No other parameters in the semi-analytical method were changed to incorporate the non-zero velocity approximation. We then run a series of convergence tests to ensure that the numerical solution computed by the semi-analytical method has converged. This convergence was achieved by $\Delta\sigma = 0.01$ and

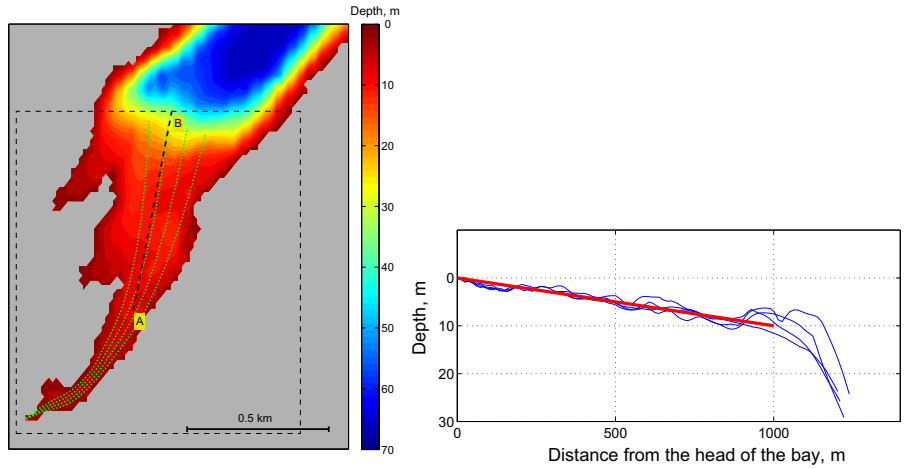

Figure 6

Left depth contours of the bathymetry of Shotgun cove. *Dotted lines* are used to generate the sample bathymetry shown in the *right* figure. *Right* Bathymetry along the *dotted green lines* (*blue*) vs. bay slope approximation (*red*)

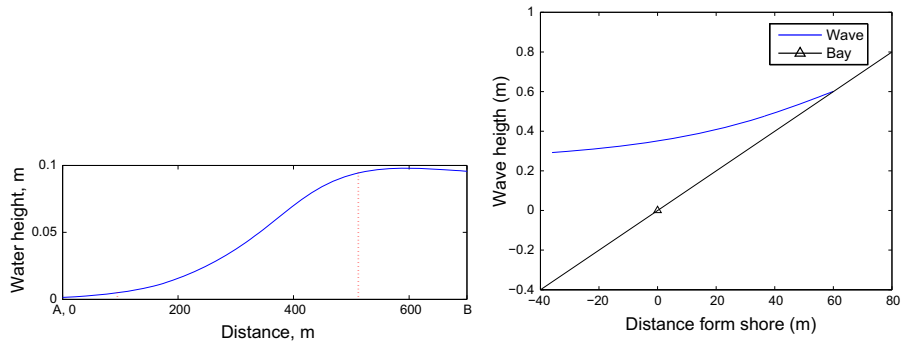

Figure 7
Left initial profile used in the realistic models. *Right* maximum run-up of the idealized experiment. Note the initial profile that was used for the idealized experiment has the same shape and amplitude as the initial profile used in the realistic models

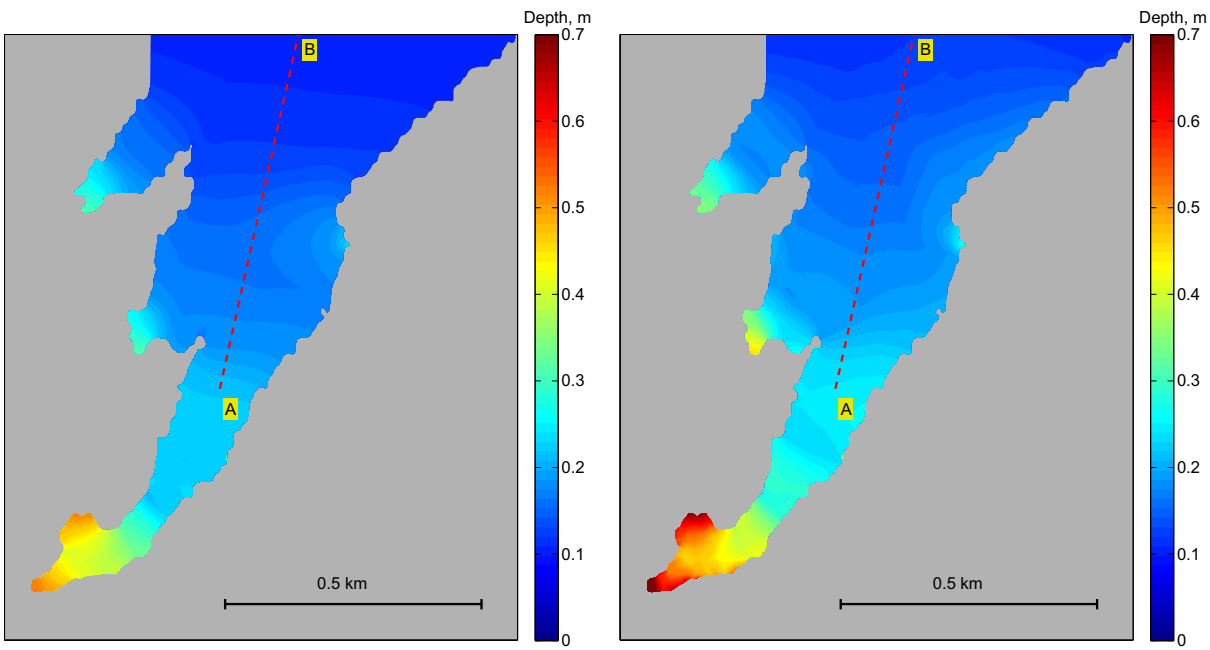

Figure 8
The maximum run-up in the realistic experiments. *Left* results obtained while using the FUNWAVE model without dispersive terms. *Right* results obtained while using the FUNWAVE model with dispersive terms

$\Delta\lambda = 0.00003$. The simulated wave profile at the maximum runup is shown in Fig. 7. Note that the computed runup is about 0.53 m. This is in good agreement with the realistic numerical experiment without dispersion considering the simplifications that go into the semi-analytical model. It is worth mentioning that the computational time required to execute the developed numerical model is just a few minutes.

Finally, in the right plot of Fig. 8 we show the computed maximum wave height in the realistic experiment with dispersion. The maximum computed runup is 0.7 or 0.2 m larger than the one obtained in the realistic experiment without dispersion. However, the discrepancy between the fully dispersive simulation of the runup and the idealized simulation is only 0.17 m.

7. Conclusions

In this paper, we develop a numerical method to implement the recent generalization of the Carrier–Greenspan transformation by Rybkin *et al.* (2014). We first present the reader with a concise overview of the recent generalization of the Carrier–Greenspan transformation. This generalization is valid for inclined bays with arbitrary cross-sections, and transforms the 1-D nonlinear shallow water wave equations into a linear second order wave equation with potential.

A finite difference method for solving the generalized Carrier–Greenspan transformation is then developed by examining the analytic properties of the transform in order to identify potential complications. As we showed, the main difficulty when numerically implementing the generalized Carrier–Greenspan transform is a strong shoreline singularity in the resulting linear wave equation. This singularity is avoided in the following two steps: first, we use the Newton-Raphson method to accurately compute the critical functions F and W in order to limit the error near the singularity, and, second, we select an appropriate finite difference scheme to handle the boundary at the moving shoreline.

To test the validity of our numerical algorithm we first consider the case of wave runup in parabolic bays as there is a known analytic solution for the runup in these cases (Didenkulova and Pelinovsky 2011b). Results of these tests show that our method generates solutions consistent with the known analytic solutions.

We then turned our attention to development of a scheme for trapezoidal bays. The current realization of the proposed numerical scheme is both robust and efficient. The code efficiency is demonstrated by comparing the computational results of our model with the results of FUNWAVE. For our model, we used an idealized trapezoidal bathymetry profile that approximates the realistic bathymetry profile used in FUNWAVE.

Our comparison reveals that the most important characteristics, such as minimum run-down and maximum run-up, are captured by the proposed numerical scheme. There are also some discrepancies between the proposed numerical scheme and FUNWAVE. The most notable of which is the difference in wave dynamics between the minimum run-down and maximum run-up. This can be seen in the third and fifth pictures in Fig. 5. The differences between the models are probably due to the de-dimensionalization of the semi-analytic method. Some preliminary modeling results of several incident N-waves show promising results in predicting the runup, but further studies are necessary.

One of the limitations of the proposed algorithm is the fact that the generalized Carrier–Greenspan transformation is not applicable to waves once they break, i.e., when the Jacobian in (10) vanishes. In case of real geophysical tsunamis, the wave length is typically rather long and thus the Jacobian may not vanish in these cases.

Even though such waves tend have an appropriate length for our method to work, the length of the entire wave train may span several different "sloping" segments of the bay. As of the writing of this paper, our model has not been adapted to model such a situation. Despite this current limitation, it is possible to model wave runup in a bay defined by multiple piece-wise segments by using a method similar to the approach in Kanoglu and Synolakis (1998). This would enable modeling of wave runup at the head of such a bay, but this is a topic for the future research and is beyond the scope of this manuscript.

Acknowledgments

This work was done as part of the REU program run by the fourth author in the summer of 2012, and was supported by NSF grant DMS 1009673. The government support is highly appreciated. We are grateful to the following other participants who also contributed to this project: Jeremiah Harrington, Lander Ver Hoef, and Viacheslav Garayshin. DJ acknowledges support from the Cooperative Institute for Alaska Research with funds from the National Oceanic and Atmospheric Administration under cooperative agreement NA08OAR4320751 with the University of Alaska. EP acknowledges support from State Contract 2014/133, RFBR grant (14-05-00092), and VolkswagenStiftung.

References

Benz, H., Dart, R., Nor, A. V., Hayes, G., Tarr, A., Furlong, K., Rhea, S., 2011. Seismicity of the earth 1900 2010 aleutian arc and vicinity. Open-file report 2010 083-b, U.S. Geological Survey, scale 1:5,000,000.

Caldwell, R., Eakins, B., Lim, E., 2009. Digital elevation models of Prince William Sound, Alaska-procedures, data sources and analysis. Tech. rep., National Geophysical Data Center, NOAA, Boulder, Colorado,http://www.ngdc.noaa.gov/dem/report/download/1305 .

Carrier, G., Greenspan, H., 1958. *Water waves of finite amplitude on a sloping beach*. Journal of Fluid Mechanics *01*, 97–109.

Courant, R., Friedrichs, K., Lewy, H., 1928. *Über die partiellen differenzengleichungen der mathematischen physic*. Mathematische Annalen *100*, 32–74.

Didenkulova, I., 2013. *Tsunami runup in narrow bays: the case of Samoa 2009 tsunami*. Natural Hazards *65*(3), 1629–1636.

Didenkulova, I., Pelinovsky, E., 2011a. *Non-linear wave evolution and run-up in an inclined channel of a parabolic cross-section*. Physics of Fluids *23*, 086602.

Didenkulova, I., Pelinovsky, E., 2011b. *Runup of tsunami waves in U-shaped bays*. Pure and Applied Geophysics *168*, 1239–1249.

Dunbar, P., Weaver, C., 2008. US states and territories. national tsunami hazard assessment: Historical record and sources for waves. Tech. rep., NOAA and USGS, 59 pp.

Ewing, L., 2011. The Tohoku tsunami of March 11, 2011: A preliminary report on effects to the California coast and planning implications. Tech. rep., California Coastal Commission, 40 pp.

Fletcher, C., 1991. Computational Techniques for Fluid Dynamics 1. Springer-Verlag, 401 pp.

Fritz, H., Borrero, J., Synolakis, C., Okal, E., Weiss, R., Lynett, P., Titov, V., Foteinis, S., Jaffe, B., Liu, P.-F., Chan., I.-C., 2011a. *Insights on the 2009 south pacific tsunami in samoa and tonga from field surveys and numerical simulations*. Earth Science Review *107*, 66–75, doi:10.1016/j.earscirev.2011.03.004.

Fritz, H., Petroff, C., Catalan, P., Cienfuegos, R., Winckler, P., Kalligeris, N., Weiss, R., Barrientos, S., Meneses, G., Valderas-Bermejo, C., Ebeling, C., Papadopoulos, A., Contreras, M., Almar, R., D. J., Synolakis, C., 2011b. *Field survey of the 27 february 2010 chile tsunami*. Pure Appl. Geophys *168*(11), 1989–2010, doi:10.1007/s00024-011-0283-5.

Garayshin, V., 2013. Tsunami runup in u and v shaped bays. Master's thesis, University of Alaska Fairbanks.

Gottlieb, S., Shu, C.-W., Tadmore, E., 2001. *Strong stability-preserving high-order time discretization methods*. SIAM Review *43*(1), 89–112.

Gusiakov, V., Marchuk, A., Osipova, A., 1997. Perspectives on Tsunami Hazard Reduction. Kluwer Academic Publishers, Ch. Expert tsunami database for the Pacific: motivation, design and proof-of-concept demonstration, pp. 21–43, available at http://tsun.sscc.ru/tsulab/On_line_Cat.htm

Kanoglu, U., 2004. *Nonlinear evolution and runup and rundown of long waves over a sloping beach*. Journal of Fluid Mechanics *513*, 363–372.

Kanoglu, U., Synolakis, C. E., 1998. *Long wave runup on piecewise linear topographies*. Journal of Fluid Mechanics *374*, 1–28.

Kanoglu, U., Synolakis, C. E., 2006. *The initial value problem solution of nonlinear shallow-water wave equations*. Physical Review Letters *97*, 148501.

Kiffer, D., October 30 2012. We all survived the great tsunami alert of 2012! SitNews: Column, http://www.sitnews.us/DaveKiffer/103012_kiffer.html

Kim, D., Kim, K., Pelinovsky, E., Didenkulova, I., Choi, B., 2013. *Three-dimensional tsuna-mi runup simulation at the Koborinai port, Sanriku coast, Japan*. Journal of Coastal Research *65*, 266–271.

Liu, H., Shimozono, T., Takagawa, T., Okayasu, A., Fritz, H., Sato, S., Tajima, Y., 2013. *The 11 March 2011 tohoku tsunami survey in rikuzentakata and comparison with historical events*. Pure Appl. Geophys *170*(6–8), 1033–1046, doi:10.1007/s00024-012-0496-2.

MATLAB, 2011. version 7.13.0.564 (R2011b). The MathWorks Inc., Natick, Massachusetts.

NGDC, 2013. National Geophysical Data Center / (NGDC/WDS) global historical tsunami database. Tech. rep., NGDC, Boulder, CO, USA, available at http://www.ngdc.noaa.gov/hazard/tsu_db.shtml

Pelinovsky, E., Troshina, E., 1994. *Propagation of long waves in straits*. Phys. Oceanography *5*, 43–48.

Ruppert, N., Lees, J., Kozyreva, N., 2007. Volcanism and Subduction: The Kamchatka Region. vol. 172 of Geophysical Monograph Series. American Geophysical Union, Washington, D.C., Ch. Seismicity, Earthquakes and Structure Along the Alaska-Aleutian and Kamchatka-Kurile Subduction Zones: A Review, pp. 129–144.

Rybkin, A., Pelinovsky, E., Didenkulova, I., 2014. *Non-linear wave run-up in bays of arbitrary cross-section:generalization of the Carrier-Greenspan approach*. Journal of Fluid Mechanics *748*, 416–432.

Shi, F., Kirby, J., Harris, J., Geiman, J., Grilli, S., 2012.*A high-order adaptive time-stepping tvd solver for boussinesq modeling of breaking waves and coastal inundation*. Ocean Modeling 43–44, 36–51.

Shimozono, T., Cui, H., Pietrzak, J., Fritz, H., Okayasu, A., Hooper, A., 2014.*Short wave amplification and extreme runup by the 2011 tohoku tsunami*. Pure Appl. Geophys. doi: 10.1007/s00024-014-0803-1 (online first, in press).

Shimozono, T., Sato, S., Okayasu, A., Tajima, Y., Fritz, H., Liu, H., Takagawa, T., 2012.*Propagation and inundation characteristics of the 2011 Tohoku Tsunami on the Central Sanriku Coast*. Coastal Eng. J *54*(1):1250004, doi:10.1142/S0578563412500040.

Stoker, J., 1957. Water waves: The Mathematical Theory with Applications. Interscience Publishers.

Synolakis, C., 1987. *The runup of solitary waves*. Journal of Fluid Mechanics *185*, 523–545.

Synolakis, C., Bernard, E., 2006. *Tsunami science before and beyond Boxing Day 2004*. Philosophical Transactions of the Royal Society A *364*, 2231–2265.

Synolakis, C., Bernard, E., Titov, V., Kanoglu, U., Gonzalez, F., 2008. *Validation and verification of tsunami numerical models*. Pure Applied Geophysics *165*, 2197–2228.

Tang, L., Titov, V., Chamberlin, C., 2009. *Development, testing, and applications of site-specific tsunami inundation models for real-time forecasting*. J. Geophys. Res. *114*, C12025, doi:10.1029/2009JC005476.

Tehranirad, B., Kirby, J., Ma, G., Shi, F., 2012a. Tsunami benchmark results for nonhydrostatic wave model NHWAVE (Version 1.1). Research report no. cacr-12-03, Center for Applied Coastal Research, University of Delaware, Newark.

Tehranirad, B., Shi, F., Kirby, J., Harris, J., Grilli, S., 2012b. Tsunami benchmark results for fully nonlinear boussinesq wave model funwavetvd, version 1.0. In: Proceedings and Results of the 2011 NTHMP Model Benchmarking Workshop. US Department of Commerce/NOAA/NTHMP, NOAA Special Report, Boulder, CO, pp. fix it, (available at http://nthmp.tsunami.gov)

Toro, E., 2009. Riemann solvers and numerical methods for fluid dynamics: a practical introduction. Springer, New York.

Wilson, R., Admire, A., Borrero, J., Dengler, L., Legg, M., Lynett, P., McCrink, T., Miller, K., Ritchie, A., Sterling, K., Whitmore, P., 2013. *Observations and impacts from the 2010 Chilean and 2011 Japanese tsunamis in California (USA)*. Pure and Applied Geophysics *170*, 1127–1147.

Wilson, R., Miller, K., 2014. Tsunami emergency response playbooks. Special report, California Geological Survey.

(Received June 20, 2014, revised November 22, 2014, accepted December 13, 2014, Published online January 15, 2015)